Reconfigurable Intelligent Surface-based Propagation Control in FBMC/OQAM Systems

Radhashyam Patra and Arunanshu Mahapatro

Veer Surendra Sai University of Technology Burla, Odisha, India

https://doi.org/10.26636/jtit.2024.1.1326

Abstract — In this paper, transmission of filter bank multicarrier (FBMC) modulated signal through reconfigurable intelligent surfaces (RIS) is proposed as an assuring technique for future wireless communication. RIS deliberately alters phases of incident signals to enhance quality of the received signal. Simulation outcomes show that it is possible to establish RIS-based FBMC communications in which RIS functions as an intelligent reflector with information concerning channel phases. It is observed that RIS-based FBMC transmissions may be a prospective solution for beyond 5G communication.

Keywords — beamforming, FBMC, MIMO, NOMA, OFDM, OQAM, RIS, terahertz

1. Introduction

Orthogonal frequency division multiplexing (OFDM) is a technology that excels among all other multicarrier modulation schemes because of its ease of implementation, lower computational complexity and higher immunity to multipath fading channel [1]. However, the out-of-band (OB) power loss caused by pulse spreading in the frequency domain and spectral loss resulting from the compulsory use of a cyclic prefix (CP) in OFDM stimulate the evolution of the scheme aiming to overcome the abovementioned issues.

To confirm the diverse use cases planned in future generation wireless communication solutions, a whippy allotment of unused time-frequency resources is needed, as depicted in Fig. 1 [2]. Discussions are currently ongoing within research groups and standardization bodies regarding the selection of the modulation technique to be relied upon in 5G wireless communications and beyond. Modified OFDM may be used for future wireless communication solutions [3]. It is also important, however, to explore alternate modulation techniques, because modulation is the foundation of any communication system that specifies affirmed uses.

In this article, the filter-bank multi-carrier (FBMC) technique [4], [5] is chosen as an alternate modulation scheme for a modified OFDM approach, as it offers much better spectral properties. FBMC can be used in many practical applications, such as cosine modulated multitone (CMT) [6], filtered multitone modulation (FMT) [7], or offset quadrature amplitude modulation (OQAM) [8], also known as staggered multitone (SMT) [9].

However, FBMC-OQAM is chosen in this article, as it supports the maximum spectral efficiency. While FBMC supports only real symbol orthogonality, some researchers rely on pulse amplitude modulation (PAM) with FBMC [7]. Two important issues have been identified for next generation communication systems, which impact the process of contriving the right modulation technique:

- whippy time-frequency resource allocation for effective affirmation of diverse user demands and channel features,
- lower delay spread, particularly in heavy heterogeneous networks relying on multiple input multiple output (MIMO) beamforming and high-carrier frequencies.

The aforementioned issues are addressed by FBMC, which seems to be a prospective choice for next generation communication solutions, due to the following reasons.

- FBMC tends to be characterized by sound localization in the time-frequency domain, permitting an effective allotment of the unused time-frequency resources,
- in the most practical scenarios, the lower delay spread ensures that only one tap equalizer is sufficient to obtain a near optimal performance [10].

Thanks to this, without loss of generality, we can approximate that FBMC symbols are interfered by first-order neighboring symbols only. However, OFDM symbols are interfered by higher-order neighboring symbols. Theoretically, this order is infinite in OFDM, while FBMC supports real signal transmission only. Also, intrinsic imaginary interference is a major hindrance in FBMC. Some of the pulse shaping filters that are widely used in FBMC include the following: extended Gaussian function (EGF), Bellanger's PHYDYAS filter, and isotropic orthogonal transform algorithm (IOTA) [10]–[12].

The most widely used multicarrier modulation techniques are introduced for potential future use.

1.1. Orthogonal Frequency Division Multiplexing

The diagram shown in Fig. 2 presents the fundamental development of an OFDM system, excluding the incorporation of bit interleavers or forward error coding. The mapping of message bits into the QAM string at the transmitter is emphasized.

Once the string has been transformed from serial-to-parallel (S/P), the individual subcarriers undergo modulation through

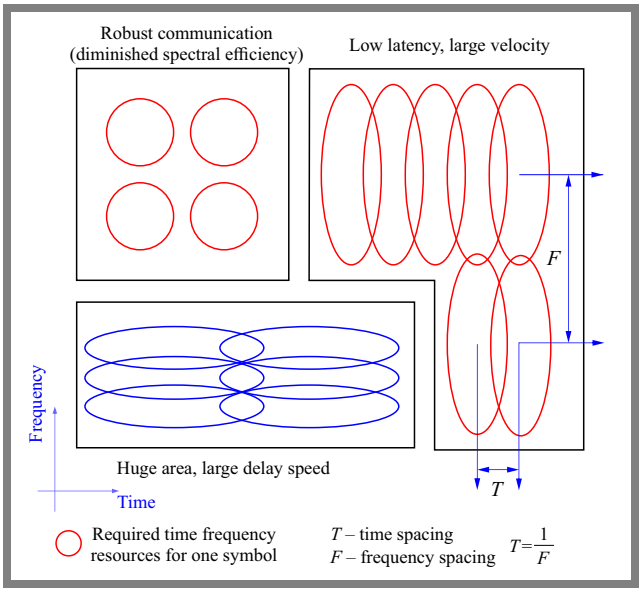

Fig. 1. Whipping allotment of time-frequency resources.

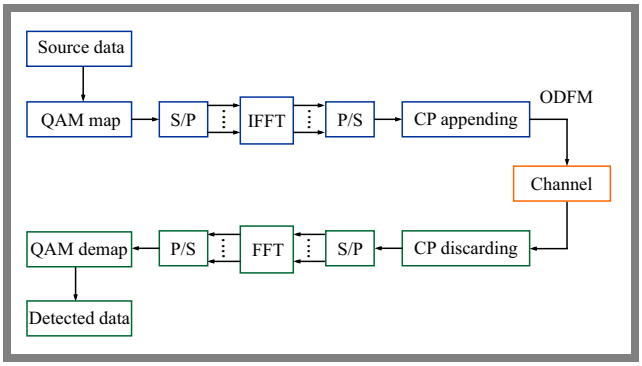

Fig. 2. Block diagram of OFDM transceiver system.

the use of IDFT. Before the transmitted signal is sent through the channel, CP is added thereto. At the receiving module, the reverse is performed. CP is initially eliminated, followed by the application of DFT for channel equalization. Thereafter, a QAM demapper is employed as the last step in contemplation of retrieving the transmitted bits.

1.2. Generalized Frequency Division Multiplexing

The field of cognitive radio makes use of generalized frequency division multiplexing (GFDM) – a digitally implemented multicarrier approach. A GFDM system satisfies the following criteria outlined in [13], [14].

- reduced OB power radiation compared to that of OFDM,
- despite the wide-band nature of GFDM, the equalization method is simple,
- frequency agility, which refers to the ability to detect and identify unused frequency bands, especially in cases when they are not sequential,
- due to the utilization of spectrum white spaces for data transmission, GFDM is not exhibiting negative interference with preexisting legacy channels.

A GFDM system is referred to as a multicarrier scheme that uses block processing.

1.3. Universal Filtered Multi-Carrier Modulation

Universal filtered multi-carrier (UFMC), sometimes also known as UF-OFDM, is another type of a multi-carrier modulation approach. The application of subband filtering that takes place in UFMC, which involves dividing the subcarriers into blocks, exhibits similarities to its implementation in GFDM. However, GFDM employs subcarrier filtering. Prior to being filtered by a prototype filter (PF) of predetermined length, every block of the subcarriers undergoes a conversion from frequency to time domain. The generation of the overall transmitted baseband signal is achieved through the superposition of subbands that have been filtered [15].

1.4. Bi-orthogonal Frequency-Division Multiplexing

Upcoming 5G specifications provide for asynchronous access, making them significantly dependent on irregular traffic. The waveform commonly used for this type of traffic is known as bi-orthogonal frequency-division multiplexing (Bi-OFDM). The Bi-OFDM scheme requires the use of pairwise orthogonality for both transmit and receive pulses – in contrast to OFDM which relies on individual orthogonality.

Nevertheless, there is a lack of matching between the filters employed in the transmitter and receiver. According to the study conducted in [16], the use of Bi-OFDM has been found to offer many advantages. As an illustration, it is more resistant to frequency offset, which puts a cap on the duration of OFDM signal.

Furthermore, the use of Bi-OFDM allows for the transmission of data on frequencies that are not currently being used, i.e. those designated as guard bands. This approach offers a balanced and controllable compromise between the degradation of performance caused by time and frequency offsets.

1.5. Filter Bank Multicarrier

The use of per-subcarrier filters in FBMC has resulted in significant enhancements to the properties of the transmitted signal. Numerous researchers have conducted investigations and showed that the choice of filters has a significant effect on the functioning of the system. Although all of these systems share the per-subcarrier filter deployment, they use distinct implementation approaches and have slightly different filter specifications. The three distinct categories of FBMC are presented below.

Cosine-modulated multitone (CMT) was first introduced in [6]. The filter bank used in CMT is generated by complex modulation of the PF, wherein the frequency responses of these filters are obtained by shifting frequency response of PF consistently. The aforementioned assumption is the reason behind the use of the terms of cosine, as opposed to complex modulation.

FBMC-FMT modulation [7] differs from CMT in that it prevents the overlapping of subbands. This means that the PF ensures a large amount of spectrum confinement, resulting in negligible inter-symbol-interference (ISI) when compared to other noise sources. To achieve subcarrier orthogonality by spectral containment, it is necessary to employ filters that

exhibit a sharp roll-off towards the frequencies at the edges of the band. At both the transmitter and receiver, FMT is performed by employing a set of uniform filters. These filters are obtained from a PF and tuned to the required frequency range, similar to the process employed in the CMT case.

Another subset of FBMC families is FBMC-OQAM, which will serve as the foundation for the subsequent sections of this paper. The FBMC principle that has received the greatest attention in literature is FBMC-OQAM, which is also referred to as SMT [9]. According to the research conducted in [5], it has been shown that among the many orthogonal FBMC waveforms, FBMC-OQAM demonstrates the highest spectral efficiency level. The transmitter component of FBMCOQAM comprises a synthesis filter bank (SFB) that shares a common output and an analysis filter bank (AFB) that shares a common input. The construction of the SFB involves the derivation of all the filters of SFB through complex PF modulation. The analysis process relies on simple matched filters in order with the corresponding transmitter counterpart for each filter at a given subcarrier.

5G has opened many research fronts, such as millimeter wave communication, index modulation (IM), non-orthogonal multiple access (NOMA), terahertz communication etc. [17]. For enhancing the quality of service in wireless communication scenarios, research focuses on issues concerned with propagating signal by controlling the reflection, scattering and refraction characteristics of electromagnetic waves [18]. Changing the signature of the received signal by the use of reconfigurable antennas is a feature of IM schemes [19]. The same objective is also achieved by the implementation of reconfigurable intelligent surfaces (RIS) that control the propagation environment [20]–[22]. RIS consist of large number of compact, cheap and passive reflecting element, which reflect only the incident signal, with a suitable phase shift.

The idea behind intelligent surfaces is projected in [23] by using active frequency selective elements that control the signal coverage. As an alternative to beamforming techniques, the smart reflect array idea is presented in [24]. It is proved that the reflect array may be utilized efficiently for altering the phase of reflected waves. The quality of the received waves may be improved by adapting the phase change of every element on the reflect-array without processing the incident waves.

Building on the development of the massive MIMO concept, the RIS idea presented in [25] utilizes a complete conterminous surface for transmission and reception. [26] focuses on downlink communication through RIS to affirm multiple-users and the sum-rate is calculated. This article proposes a new physical layer communication technique using the FM-BC modulation scheme and controlling signal propagation by the use of RIS, while signal reception relies on a single antenna system.

It is worth noticing that RIS-based FBMC communication is completely different from multiple input multiple output (MIMO) FBMC [27], beamforming-FBMC [28], amplify and forward relaying FBMC [29], and backscatter FBMC communication [30]. In RIS-FBMC, large numbers of tiny, passive elements reflect the incoming FBMC wave with a controllable phase change, without using a power supply.

The contribution of this paper is highlighted below:

- we implemented the RIS-based propagation control method in FBMC/OQAM systems,
- we derived the optimum value of the phase introduced by RIS elements,
- we proved, via simulation, that the bit error rate (BER) of this system is better than the one achieved in non-RIS based FBMC systems.

Notations used: $(\cdot)^*, *$ represents conjugate, convolution respectively. $\Re(\cdot)$ and $\Im(\cdot)$ stands for real and imaginary part. a_{ij} is the i-th row and j-th column element of a matrix. $j \equiv \sqrt{-1}$. $\mathcal{N}(\mu, \sigma^2)$ and $\mathcal{CN}(\mu, \sigma^2)$ stands for a real and complex Gaussian-random-variable (GRV) with mean μ and variance σ^2 respectively.

The remainder of the paper is organized as follows. Section 2 explains the RIS-FBMC/OQAM system including the FBMC transmission model, RIS model and behavior, channel model, reception model, and data detection. In Section 3, the optimum values of RIS elements are derived. Section 4 contains an analysis of the simulation results. The paper is concluded in Section 5.

2. Transmission Model

In this paper, an RIS-based FBMC/OQAM transceiver system is considered, as shown in Fig. 3, where the signal is received after being reflected from RIS. Here, we assume – similarly as has been done in paper [21] – that no direct path exists between the transmitter and the receiver. Since RIS is considered to be an integrated part of the transmitter, the path loss between the transmitter and RIS is neglected. RIS consists of L passive reflecting elements in the form of a 2-dimensional array. The channel between the l-th reflecting element of RIS and the receiving antenna is modeled as:

$$h_l = \beta_l \mathrm{e}^{-\mathrm{j}\psi_l}, \tag{1}$$

where $l = \{1, \ldots, L\}$, β_l is the magnitude and ψ_l is the phase. Here, we assume the channel is flat fading with h_l to be circularly-symmetric complex GRV having mean zero and variance 1. The l-th RIS element introduces a phase shift of ϕ_l to the incident signal [21].

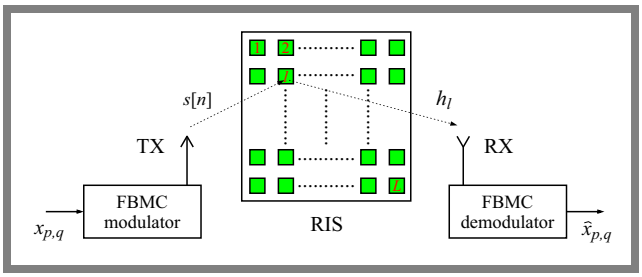

Fig. 3. RIS-based propagation controlled FBMC/OQAM system model.

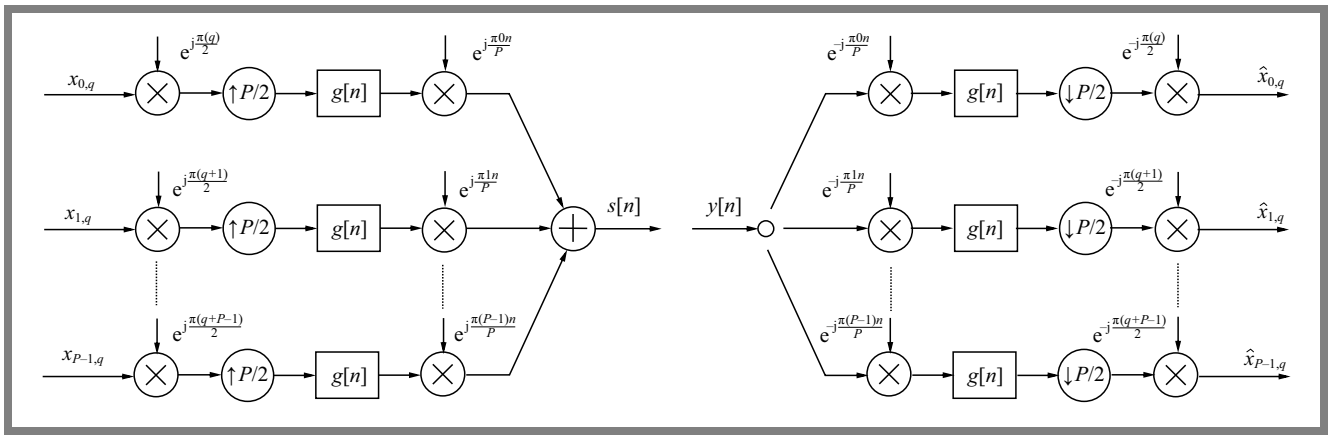

Fig. 4. FBMC/OQAM transceiver system.

2.1. RIS-FBMC/OQAM System Model

The FBMC/OQAM system considered in this article (Fig. 4) contains P sub-channels with a sub-channel guard band of $1/T_s$, where T_s stands for the complex symbol duration. The FBMC transmitted signal at the n-th sample index is given by [1]:

$$s[n] = \sum_{p=0}^{P-1} \sum_{q\in\mathbb{Z}} x_{p,q}\chi_{p,q}[n]\,, \tag{2}$$

where p and q denote the sub-channel index and the real OQAM symbol index, respectively.

The FBMC basis function $\chi_{p,q}[n]$ is defined as:

$$\chi_{p,q}[n] = \mathrm{e}^{\mathrm{j}\phi_{p,q}}\mathrm{e}^{\frac{\mathrm{j}2\pi pn}{P}} g\left[n - q\frac{P}{2}\right], \tag{3}$$

where $g[n]$ is the impulse response of the PF. This filter has real and symmetric coefficients and unit energy which ensures that the energy of the input signal remains unchanged [4]. Filter length is $L_g = bP$ with overlapping factor b. $\phi_{p,q} = \frac{\pi}{2}(p+q) - \pi pq$ denotes the phase factor for the p-th sub-channel and the q-th OQAM symbol instant. The symbol corresponding to the p-th sub-channel and the q-th real OQAM symbol index is denoted as $x_{p,q}$ and is obtained from the complex constellation symbols $z_{p,q}$ as:

$$x_{p,2q} = \begin{cases} \Re\{z_{p,q}\}, & \text{when } p \text{ is even} \\ \Im\{z_{p,q}\}, & \text{when } p \text{ is odd} \end{cases}$$
$$x_{p,2q+1} = \begin{cases} \Im\{z_{p,q}\}, & \text{when } p \text{ is even} \\ \Re\{z_{p,q}\}, & \text{when } p \text{ is odd} \end{cases}. \tag{4}$$

In this system model, the FBMC modulated signal $s[n]$ is reflected by the elements of RIS and then each reflected signals is intercepted at the receiving module. The received signal $y[n]$ at the n-th sample index is:

$$y[n] = \left[\sum_{l=1}^{L} h_l \mathrm{e}^{\mathrm{j}\phi_l}\right] s[n] + w[n]\,, \tag{5}$$

where white Gaussian noise $w[n]$ is distributed as $\mathcal{CN}(0,\sigma_w^2)$. Below, we discuss the effect of RIS on detecting the transmitted data $x_{p,q}$ using the received signal $y[n]$.

2.2. Effect of RIS on FBMC Demodulation

Here, we consider the matched filter-based detection method [1] for a RIS-assisted FBMC-OQAM system. The FBMC demodulated signal at the $\bar{p}$-th subchannel and $\bar{q}$-th OQAM symbol instant $y_{\bar{p},\bar{q}}$ is obtained as:

$$y_{\bar{p},\bar{q}} = \sum_{n=0}^{\infty} y[n]\chi^*_{\bar{p},\bar{q}}[n]\,. \tag{6}$$

We simplify this using Eq. (5) as:

$$\begin{aligned}
y_{\bar{p},\bar{q}} &= \sum_{n=0}^{\infty}\left\{\left[\sum_{l=1}^{L} h_l \mathrm{e}^{\mathrm{j}\phi_l}\right] s[n] + w[n]\right\}\chi^*_{\bar{p},\bar{q}}[n] \\
&= \sum_{n=0}^{\infty}\left\{\left[\sum_{l=1}^{L} h_l \mathrm{e}^{\mathrm{j}\phi_l}\right] s[n]\right\}\chi^*_{\bar{p},\bar{q}}[n] + \sum_{n=0}^{\infty} w[n]\chi^*_{\bar{p},\bar{q}}[n] \\
&= \left[\sum_{l=1}^{L} h_l \mathrm{e}^{\mathrm{j}\phi_l}\right]\left\{\sum_{n=0}^{\infty} s[n]\chi^*_{\bar{p},\bar{q}}[n]\right\} + \sum_{n=0}^{\infty} w[n]\chi^*_{\bar{p},\bar{q}}[n] \\
&= \sum_{l=1}^{L} h_l \mathrm{e}^{\mathrm{j}\phi_l}\left[\sum_{n=0}^{\infty}\sum_{p=0}^{P-1}\sum_{q\in\mathbb{Z}} x_{p,q}\chi_{p,q}[n]\chi^*_{\bar{p},\bar{q}}[n]\right] \\
&\quad + \sum_{n=0}^{\infty} w[n]\chi^*_{\bar{p},\bar{q}}[n] \\
&= \sum_{l=1}^{L} h_l \mathrm{e}^{\mathrm{j}\phi_l}\left[\sum_{p=0}^{P-1}\sum_{q\in\mathbb{Z}} x_{p,q}\left(\sum_{n=0}^{\infty}\chi_{p,q}[n]\chi^*_{\bar{p},\bar{q}}[n]\right)\right] \\
&\quad + \sum_{n=0}^{\infty} w[n]\chi^*_{\bar{p},\bar{q}}[n] \\
&= \sum_{l=1}^{L} h_l \mathrm{e}^{\mathrm{j}\phi_l}\left[\sum_{p=0}^{P-1}\sum_{q\in\mathbb{Z}} x_{p,q}\xi^{\bar{p},\bar{q}}_{p,q}\right] + \eta_{\bar{p},\bar{q}}\,,
\end{aligned} \tag{7}$$

where the trans-multiplexer function $\xi^{\bar{p},\bar{q}}_{p,q}$ and the effective noise $\eta_{\bar{p},\bar{q}}$ are defined as: $\xi^{\bar{p},\bar{q}}_{p,q} = \sum_{n=0}^{\infty}\chi_{p,q}[n]\chi^*_{\bar{p},\bar{q}}[n]$, and $\eta_{\bar{p},\bar{q}} = \sum_{n=0}^{\infty} w[n]\chi^*_{\bar{p},\bar{q}}[n]$. The distribution of $\eta_{\bar{p},\bar{q}}$ remains almost the same as that of $w[n]$. This is so because the $n = 0$

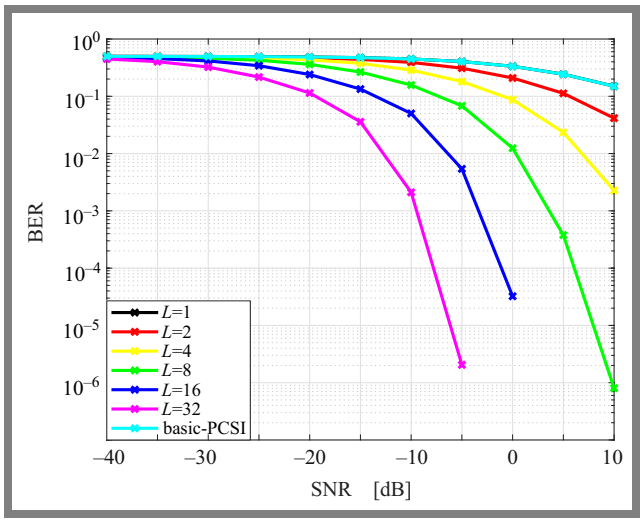

Fig. 5. BER comparison of RIS-FBMC/OQAM and FBMC/OQAM systems for a 64QAM flat-fading channel.

prototype filter $g[n]$ and thus $\chi_{p,q}[n]$ does not alter energy of the input signal and is of the sharp variety [4]. It is also known that [1]:

$$\xi_{p,q}^{\bar{p},\bar{q}} = \begin{cases} 1, & \text{if } (p,q) = (\bar{p},\bar{q}) \\ j\langle\xi\rangle_{p,q}^{\bar{p},\bar{q}}, & \text{if } (p,q) \neq (\bar{p},\bar{q}) \end{cases}, \tag{8}$$

where $\langle\xi\rangle_{p,q}^{\bar{p},\bar{q}} = \Im\left\{\sum_{n=0}^{\infty} \chi_{p,q}[n]\chi_{\bar{p},\bar{q}}^{*}[n]\right\}$ represents the imaginary part of the trans-multiplexer function. Now, by substituting Eq. (8) to Eq. (7), we obtain:

$$\begin{aligned} y_{\bar{p},\bar{q}} &= \left[\sum_{l=1}^{L} h_l \mathrm{e}^{\mathrm{j}\phi_l}\right]\left\{x_{\bar{p},\bar{q}}\xi_{\bar{p},\bar{q}}^{\bar{p},\bar{q}} + \sum_{\substack{p=0,\\ p\neq\bar{p}}}^{N-1}\sum_{\substack{q\in\mathbb{Z},\\ q\neq\bar{q}}} x_{p,q}\xi_{p,q}^{\bar{p},\bar{q}}\right\} + \eta_{\bar{p},\bar{q}} \\ &= \mathrm{j}\left[\sum_{l=1}^{L}\beta_l \mathrm{e}^{-\mathrm{j}(\psi_l-\phi_l)}\right]\left\{\sum_{(p,q)\neq(\bar{p},\bar{q})} x_{p,q}\langle\xi\rangle_{p,q}^{\bar{p},\bar{q}}\right\} + \\ &\quad \left[\sum_{l=1}^{L}\beta_l \mathrm{e}^{-\mathrm{j}(\psi_l-\phi_l)}\right] x_{\bar{p},\bar{q}} + \eta_{\bar{p},\bar{q}}\,, \end{aligned} \tag{9}$$

where Eq. (9) follows Eq. (1). The real QAM symbol $x_{p,q}$ can be detected by extracting the real part of Eq. (9), i.e.:

$$\hat{x}_{p,q} = \Re\{y_{\bar{p},\bar{q}}\}\,. \tag{10}$$

We observe from Eqs. (9) and (12) that the values of the phases of RIS elements $\{\phi_l\}_{l=1,\ldots,L}$ play a major role in reliable detection of the transmitted signal $x_{\bar{p},\bar{q}}$. Therefore, we need to find the optimal values of phases $\{\phi_l\}_{l=1,\ldots,L}$ by maximizing the instantaneous SNR which, in turn, will minimize BER.

3. Optimal Values of the Phases of RIS Elements

The second term in Eq. (9) contains the necessary data part $x_{\bar{p},\bar{q}}$, the first term contains the intrinsic interference $\left\{\sum_{(p,q)\neq(\bar{p},\bar{q})} x_{p,q}\langle\xi\rangle_{p,q}^{\bar{p},\bar{q}}\right\}$ and the third term is the effective noise. The intrinsic interference can be completely removed by taking the real part of Eq. (9), if and only if the term $\left[\sum_{l=1}^{L}\beta_l \mathrm{e}^{-\mathrm{j}(\psi_l-\phi_l)}\right]$ is real. From Eq. (1) we know that β_l and ψ_l are, respectively, the magnitude and phase of the channel between the l-th element of RIS and the receiver, and ϕ_l is the phase introduced by the l-th element of RIS. The term $\left[\sum_{l=1}^{L}\beta_l \mathrm{e}^{-\mathrm{j}(\psi_l-\phi_l)}\right]$ can be made real if and only if $(\psi_l - \phi_l) = 2K\pi$, where K is an integer.

However, if $K \neq 0$, then the phase to be introduced by the RIS elements will be $\phi_l = \psi_l - 2K\pi$. For this subtraction operation, RIS will consume more power and will demand computational complexity which will negate the principle according to which RIS is consuming much less power than other methods, such as those relying on the use of a power amplifier etc. For other values, the overall phase summation may also go to zero for a very large value of L, as the channel's complexity coefficient is a random variable with a zero mean. However, in practice, the number of RIS elements L is considered to equal 2, 4, 8, 16, and 32. With this value of L, the aforementioned summation will not be zero in practice. Hence, we consider $K = 0$, i.e. $\phi_l = \psi_l$. It is also assumed that the reflecting surface is intelligent, i.e. the surface possess the knowledge of channel phase ψ_l and, according thereto, the surface makes the phase introduced by its elements ϕ_l equal and opposite in polarity to ψ_l, (i.e. reconfigurable), so that the term $\left[\sum_{l=1}^{L}\beta_l \mathrm{e}^{-\mathrm{j}(\psi_l-\phi_l)}\right]$ becomes real and can be expressed as:

$$\left[\sum_{l=1}^{L}\beta_l \mathrm{e}^{-\mathrm{j}(\psi_l-\phi_l)}\right] = \sum_{l=1}^{L}\beta_l = B\,, \tag{11}$$

where B is a real constant and is > 1. Therefore, Eq. (9) can be represented as:

$$y_{\bar{p},\bar{q}} = Bx_{\bar{p},\bar{q}} + \mathrm{j}B\left\{\sum_{(p,q)\neq(\bar{p},\bar{q})} x_{p,q}\langle\xi\rangle_{p,q}^{\bar{p},\bar{q}}\right\} + \eta_{\bar{p},\bar{q}}. \tag{12}$$

By taking the real part of Eq. (12), we obtain:

$$y_{\bar{p},\bar{q}} = Bx_{\bar{p},\bar{q}} + \Re\{\eta_{\bar{p},\bar{q}}\}. \tag{13}$$

The factor B in Eq. (13) is the contribution of RIS that enhances SNR in the RIS-FBMC system, which is derived next. Hence, BER is also improved.

We can otherwise prove the same as follows. Considering that the instantaneous energy of an FBMC-modulated signal $s[n]$ is E_n, the instantaneous SNR at the receiving antenna is

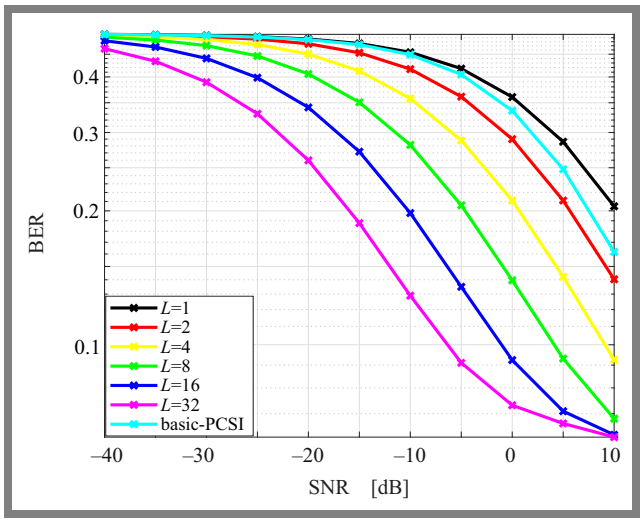

Fig. 6. BER comparison of RIS-FBMC/OQAM and FBMC/OQAM systems for a 64QAM frequency selective-fading channel.

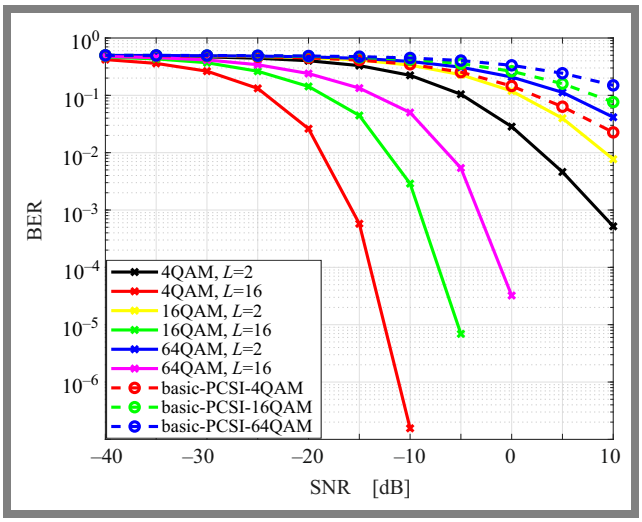

Fig. 7. BER comparison of RIS-FBMC/OQAM and FBMC/OQAM systems for different QAM and flat-fading channels.

given as:

$$\text{ISNR} = \frac{E_n \left| \sum_{l=1}^{L} \beta_l \mathrm{e}^{\mathrm{j}(\phi_l - \psi_l)} \right|^2}{\sigma_w^2}. \tag{14}$$

Now, we can maximize ISNR by maximizing $\left| \sum_{l=1}^{L} \beta_l \mathrm{e}^{\mathrm{j}(\phi_l - \psi_l)} \right|^2$ as:

$$\begin{aligned} \left| \sum_{l=1}^{L} \beta_l \mathrm{e}^{\mathrm{j}(\phi_l - \psi_l)} \right|^2 &= \left| \sum_{l=1}^{L} \beta_l \mathrm{e}^{\mathrm{j}\theta_l} \right|^2 \\ &= \sum_{l=1}^{L} \{\beta_l\}^2 + 2 \sum_{l=1}^{L} \sum_{k=l+1}^{L} \beta_l \beta_k \cos(\theta_l - \theta_k). \end{aligned} \tag{15}$$

where $\theta_l = \phi_l - \psi_l$. We know that Eq. (15) reaches its maximum when $\theta_l - \theta_k = 0$, i.e. $\theta_l = \theta_k$. Otherwise, we can say that the resultant phase of each reflected signal after the phase introduced by the respective reflecting element must be the same.

Assume that:

$$\begin{aligned} \theta_l &= \theta_k = c \\ \Rightarrow \phi_l - \psi_l &= \phi_k - \psi_k = c \\ \Rightarrow \phi_l = c + \psi_l, &\qquad \phi_k = c + \psi_k \,, \end{aligned} \tag{16}$$

where c is a constant phase.

The reflecting elements we have considered are smart, meaning they have the knowledge of the phase of the corresponding channel. It is clear from Eq. (16) that if $c \neq 0$, then each reflecting element requires one extra addition to reconfigure the phase it introduces, namely ϕ_l. This, in turn, demands extra circuitry and power. So, to avoid these overheads, we chose $c = 0$, i.e. the elements introduce a phase equal and opposite to the corresponding channel phase $\phi_l = -(\psi_l)$. This makes the resultant phase of signal from each element zero and equal. Therefore, we can express ISNR as:

$$\text{ISNR} = \frac{E_n \left| \sum_{l=1}^{L} \beta_l \right|^2}{\sigma_w^2} = \frac{E_n B^2}{\sigma_w^2}; \; B > 1. \tag{17}$$

Below, the effective SNR of the detected symbol is to be derived. In Eq. (13), the first term contains the necessary data symbol, the second term is the noise added to the channel. Hence, effective SNR of a RIS-based FBMC/OQAM system is given as:

$$\text{SNR}_{\text{eff}}^{\text{RIS-FBMC}} = \frac{B^2 \sigma_x^2}{\frac{1}{2}\sigma_w^2} = \frac{2B^2 \sigma_x^2}{\sigma_w^2}; \; B > 1 \,, \tag{18}$$

where σ_x^2 is the variance of each real OQAM symbol $x_{\bar{p},\bar{q}}$, σ_w^2 is the variance of complex AWGN added to the channel and the factor of $1/2$ used in the noise part results from the assumption that complex noise power is equally split between its real and imaginary parts.

For an FBMC system having perfect channel state information and not relying on RIS, the effective SNR of a basic FBMC/OQAM system is given by:

$$\text{SNR}_{\text{eff}}^{\text{Basic-FBMC}} = \frac{\sigma_x^2}{\frac{1}{2}\sigma_w^2} = \frac{2\sigma_x^2}{\sigma_w^2}. \tag{19}$$

Therefore, by implementing RIS in an FBMC system, the effective SNR of the FBMC system is enhanced by a factor of B^2.

4. Simulation Results

The parameters taken into consideration in the simulation are as follows. The number of sub-channels $P = 64$, the number of OQAM symbol instants $Q = 50$, sub-channel spacing $1/T_s = 15$ kHz, the number of reflecting elements in the reconfigurable intelligent surface $L = \{1, 2, 4, 8, 16, 32\}$, and the channel tap length equals $\{1, 6\}$. The pulse-shaping-filter implemented in this article is Bellanger's PHYDYAS filter [4]. The channel coefficients are complex, with their

real and imaginary parts being independent-and-identically-distributed (i.i.d.) with $\mathcal{CN}(0,1)$. The noise added to the channel is complex AWGN, with its real and imaginary parts being i.i.d. with $\mathcal{CN}(0,\sigma_w^2)$. In the simulation, the signal power is kept at a constant level of 1 and the noise power σ_w^2 is varied as $\sigma_w^2 = 1/SNR$.

BER performance of the FBMC/OQAM system, with its propagation based on RIS, is shown in Fig. 5 for a 64QAM, flat fading channel, and different numbers of reflecting elements in RIS. Its BER is also compared with that of a basic FBMC/OQAM system with a perfect channel information scenario (PCSI) [1]. It is clear from Fig. 5 that BER performance of the FBMC/OQAM system with propagation based on RIS is better than that of a conventional FBMC/OQAM system.

The received signal in the proposed method is given in Eq. (4). The term $\left[\sum_{l=1}^{L} h_l e^{j\phi_l}\right]$ multiplied by the FBMC transmitted signal $s[n]$ is responsible for such a low BER. From Eq. (1), the channel model between the RIS element and the receiver is known. For maximized SNR at the receiver, the phase of the channel and the phase introduced by the reflecting elements are made equal and opposite in polarity. So, the cumulative effect of $\left[\sum_{l=1}^{L} h_l e^{j\phi_l}\right]$ on $s[n]$ becomes a multiplication of a real number with a magnitude greater than 1. Hence, BER performance of the system is better than that of a basic FBMC system, as the received signal power is amplified.

The value of this real number is dependent on the number of reflecting elements in the RIS. As the number of elements in RIS increases, BER performance improves as well, which is also seen in Fig. 5. By using a power amplifier in the transmitter, we can amplify the received signal, but that requires more power. However, in the RIS-based propagation control method, no dedicated power supply is needed as no RF processing is performed in RIS. The elements of RIS are just smart reflectors that consume negligible amounts of power. Figure 6 shows the BER of the proposed technique for a frequency-selective channel having a tap length of 6.

Figure 7 shows the comparison of BER of the proposed system with a varying number of reflecting elements in RIS, with that of conventional FBMC/OQAM systems with PCSI [1] for different modulation schemes and flat fading channel scenarios. Similarly, Fig. 8 compares BER for a frequency selective fading channel with a tap length of 6. It is clear from both figures that the proposed system offers superior BER performance when compared with conventional FBMC/OQAM systems in every channel scenario and each modulation scheme.

5. Conclusion and Future Work

In this article, reconfigurable intelligent surface-based propagation control in an FBMC/OQAM system is implemented. From simulations, one may observe that the BER performance of this method outperforms that of a simple FBMC/OQAM system. In addition, as the number of elements in the RIS increases, the BER improves even further. The extra power consumption stemming from implementing RIS in an FBMC system is negligible. So, the proposed scheme offers significant benefits in terms of both BER and power consumption.

In this study, RIS is regarded to be an integral component of the transmitter and the path-loss between the transmitter and RIS is neglected. In future work, it is possible to position RIS at a distance from the transmitter, hence necessitating the consideration of path-loss between the transmitter and the RIS.

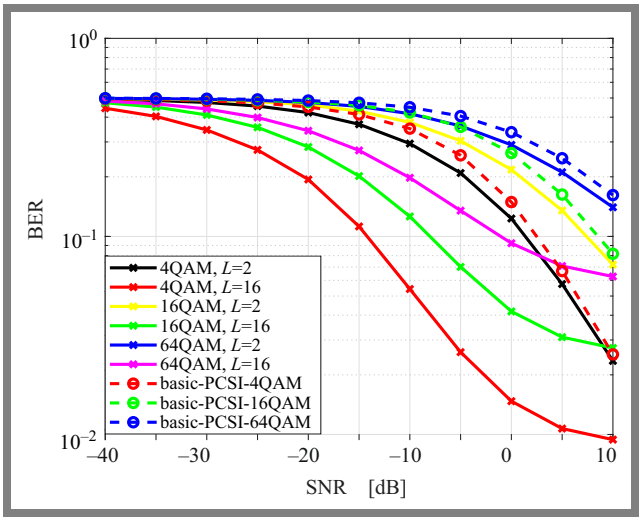

Fig. 8. BER comparison of RIS-FBMC/OQAM and FBMC/OQAM systems for different QAM and frequency selective-fading channels.

References

[1] P. Siohan, C. Siclet, and N. Lacaille, "Analysis and Design of OQAM-OFDM Systems Based on Filterbank Theory", *IEEE Transactions on Signal Processing*, vol. 50, no. 5, pp. 1170–1183, 2002 (https://doi.org/10.1109/78.995073).

[2] R. Chavez-Santiago *et al.*, "5G: The Convergence of Wireless Communications", *Wireless Personal Communication*, vol. 83, pp. 1617–1642, 2015 (https://doi.org/10.1007/s11277015-2467-2).

[3] P. Banelli *et al.*, "Modulation Formats and Waveforms for 5G Networks: Who Effect of RIS on FBMC Demodulation will be the Heir of OFDM? – An Overview of Alternative Modulation Schemes for Improved Spectral Efficiency", *IEEE Signal Processing Magazine*, vol. 31, no. 6, pp. 80–93, 2014 (https://doi.org/10.1109/MSP.2014.2337391).

[4] M. Bellanger *et al.*, *FBMC Physical Layer: A Primer*, PHYDYAS Project, 2010 (https://pdf4pro.com/view/fbmc-physical-layera-primer-phydyas-project-2a7e75.html).

[5] A. Sahin, I. Guvenc, and H. Arslan, "A Survey on Multicarrier Communications: Prototype Filters, Lattice Structures, and Implementation Aspects", *IEEE Communications Surveys and Tutorials*, vol. 16, no. 3, pp. 1312–1338, 2012 (https://doi.org/10.1109/SURV.2013.121213.00263).

[6] B. Farhang-Boroujeny, "OFDM versus Filter Bank Multicarrier", *IEEE Signal Processing Magazine*, vol. 28, no. 3, pp. 92–112, 2011 (https://doi.org/10.1109/MSP.2011.940267).

[7] G. Cherubini, E. Eleftheriou, and S. Olcer, "Filtered Multitone Modulation for VDSL", *Seamless Interconnection for Universal Services, Global Telecommunications Conference, GLOBECOM'99*, Rio de Janeiro, Brazil, 1999 (https://doi.org/10.1109/GLOCOM.1999.829951).

[8] H. Bolcskei, "Orthogonal Frequency Division Multiplexing Based on Offset QAM", in: H.G. Feichtinger, T. Strohmer, *Advances in Gabor*

Analysis, Springer, pp. 321–352, 2003 (https://doi.org/10.1007/978-1-4612-0133-5_12).

[9] A. Viholainen, M. Bellanger, and M. Huchard, "Project PHYDYAS, Deliverable 5.1: Prototype filter and structure optimization", *FP7-ICT,* Technical Report, 2009.

[10] R. Nissel, S. Schwarz, and M. Rupp, "Filter Bank Multicarrier Modulation Schemes for Future Mobile Communications", *IEEE Journal on Selected Areas in Communications*, vol. 35, no. 8, pp. 1768–1782, 2017 (https://doi.org/10.1109/JSAC.2017.2710022).

[11] M. Bellanger, "Specification and Design of a Prototype Filter for Filter Bank Based Multicarrier Transmission", *2001 IEEE International Conference on Acoustics, Speech, and Signal Processing*, Salt Lake City, USA, 2001 (https://doi.org/10.1109/ICASSP.2001.940488).

[12] J. Du, P. Xiao, J. Wu, and Q. Chen, "Design of Isotropic Orthogonal Transform Algorithm-based Multicarrier Systems with Blind Channel Estimation", *IET Communications*, vol. 6, no. 16, pp. 2695–2704, 2012 (https://doi.org/10.1049/iet-com.2012.0029).

[13] G. Fettweis, M. Krondorf, and S. Bittner, "GFDM - Generalized Frequency Division Multiplexing", *VTC Spring 2009 IEEE 69th Vehicular Technology Conference*, Barcelona, Spain, 2009 (https://doi.org/10.1109/VETECS.2009.5073571).

[14] N. Michailow *et al.*, "Generalized Frequency Division Multiplexing for 5th Generation Cellular Networks", *IEEE Transactions on Communications*, vol. 62, no. 9, pp. 3045–3061, 2014 (https://doi.org/10.1109/TCOMM.2014.2345566).

[15] T. Wild, F. Schaich, and Y. Chen, "5G Air Interface Design Based on Universal Filtered (UF-) OFDM", *2014 19th International Conference on Digital Signal Processing*, Hong Kong, China, 2014 (https://doi.org/10.1109/ICDSP.2014.6900754).

[16] M. Kasparick, G. Wunder, P. Jung, and D. Maryopi, "Bi-orthogonal Waveforms for 5G Random Access with Short Message Support", *European Wireless 2014; 20th European Wireless Conference*, Barcelona, Spain, 2014 (https://ieeexplore.ieee.org/document/6843162).

[17] A. Gatherer, "What Will 6G be?", *ComSoc Technology News (CTN)*, 2018 [Online]. Available: (https://www.comsoc.org/publications/ctn/what-will-6g-be).

[18] M. Di Renzo *et al.*, "Smart Radio Environments Empowered by Reconfigurable AI Meta-surfaces: An Idea whose Time Has Come", *EURASIP Journal on Wireless Communications and Networking*, vol. 2019, art. no. 129, 2019 (https://doi.org/10.1186/s13638-019-1438-9).

[19] Y. Naresh and A. Chockalingam, "On Media-Based Modulation Using RF Mirrors", *IEEE Transactions on Vehicular Technology*, vol. 66, no. 6, pp. 4967–4983, 2017 (https://doi.org/10.1109/TVT.2016.2620989).

[20] C. Liaskos *et al.*, "A New Wireless Communication Paradigm through Software-Controlled Metasurfaces", *IEEE Communications Magazine*, vol. 56, no. 9, pp. 162–169, 2018 (https://doi.org/10.1109/MCOM.2018.1700659).

[21] E. Basar, "Reconfigurable Intelligent Surface-Based Index Modulation: A New Beyond MIMO Paradigm for 6G", *IEEE Transactions on Communications*, vol. 68, no. 5, pp. 3187–3196, 2020 (https://doi.org/10.1109/TCOMM.2020.2971486).

[22] C. Huang, A. Zappone, G. C. Alexandropoulos, M. Debbah, and C. Yuen, "Reconfigurable Intelligent Surfaces for Energy Efficiency in Wireless Communication", *IEEE Transactions on Wireless Communications*, vol. 18, no. 8, pp. 4157–4170, 2019 (https://doi.org/10.1109/TWC.2019.2922609).

[23] L. Subrt and P. Pechac, "Controlling Propagation Environments Using Intelligent Walls", *2012 6th European Conference on Antennas and Propagation (EUCAP)*, Prague, Czech Republic, 2012 (https://doi.org/10.1109/EuCAP.2012.6206517).

[24] X. Tan, Z. Sun, J.M. Jornet, and D. Pados, "Increasing Indoor Spectrum Sharing Capacity Using Smart Reflect-array", *2016 IEEE International Conference on Communications (ICC)*, Kuala Lumpur, Malaysia, 2016 (https://doi.org/10.1109/ICC.2016.7510962).

[25] S. Hu, F. Rusek, and O. Edfors, "Beyond Massive MIMO: The Potential of Data Transmission with Large Intelligent Surfaces", *IEEE Transactions on Signal Processing*, vol. 66, no. 10, pp. 2746–2758, 2018 (https://doi.org/10.1109/TSP.2018.2816577).

[26] C. Huang, G.C. Alexandropoulos, A. Zappone, M. Debbah, and C. Yuen, "Energy Efficient Multi-user MISO Communication Using Low Resolution Large Intelligent Surfaces", *2018 IEEE Globecom Workshops (GC Wkshps)*, Abu Dhabi, UAE, 2018 (https://doi.org/10.1109/GLOCOMW.2018.8644519).

[27] J. Tellado, S. Talwar, H. Sampath, V. Erceg, and A. Paulraj, "A Fourth-generation MIMO-OFDM Broadband Wireless System: Design Performance and Field Trials Results", *IEEE Communications Magazine*, vol. 40, no. 9, pp. 143–149, 2002 (https://doi.org/10.1109/MCOM.2002.1031841).

[28] D. Qu, Y. Qiu, and T. Jiang, "Finer SVD-Based Beamforming for FBMC/OQAM Systems", *2016 IEEE Global Communications Conference (GLOBECOM)*, Washington, USA, 2016 (https://doi.org/10.1109/GLOCOM.2016.7841842).

[29] J. Zhang, A. Nimr and M. Haardt, "Joint Design of Multi-tap Filters and Power Control for FBMC/OQAM Based Two-way Decode-and-forward Relaying Systems in Highly Frequency Selective Channels", *2015 IEEE International Conference on Acoustics, Speech and Signal Processing (ICASSP)*, South Brisbane, Australia, 2015 (https://doi.org/10.1109/ICASSP.2015.7178409).

[30] S. Koslowski, M. Braun, and F.K. Jondral, "Using Filter Bank Multicarrier Signals for Radar Imaging", *2014 IEEE/ION Position, Location and Navigation Symposium – PLANS 2014*, Monterey, USA, 2014 (https://doi.org/10.1109/PLANS.2014.6851369).

Radhashyam Patra, M.Tech., Assistant Professor
Department of Electronics and Telecommunication Engineering
https://orcid.org/0000-0001-5032-9240
E-mail: radhashyampatra2211@gmail.com
Veer Surendra Sai University of Technology Burla, Odisha, India
https://www.vssut.ac.in

Arunanshu Mahapatro, Ph.D., Associate Professor
Department of Electronics and Telecommunication Engineering
https://orcid.org/0000-0002-4171-3926
E-mail: arunanshu_etc@vssut.ac.in
Veer Surendra Sai University of Technology Burla, Odisha, India
https://www.vssut.ac.in